# Arrested Tumbling in Shearing Flows of Liquid Crystal Polymers

**R. G. Larson**

*AT&T Bell Laboratories, Murray Hill, New Jersey 07974*

*Received January 29, 1990; Revised Manuscript Received March 8, 1990*

ABSTRACT: The Doi equation for the three-dimensional time-dependent orientation-distribution function for rodlike polymers in the nematic liquid crystalline state in the presence of shearing flow is solved by an expansion in spherical harmonic functions. The excluded-volume interactions between the molecules are accounted for with the Onsager potential. The results confirm two-dimensional calculations with the Maier–Saupe potential by Marrucci and Maffettone, who showed that a regime of steady-state negative first normal stress difference $N_1$ exists at shear rates high enough to frustrate the tumbling of the average molecular orientation that occurs at lower shear rates. We find in addition that the second normal stress difference $N_2$ usually is of sign opposite that of $N_1$ and is therefore positive when $N_1$ is negative. Between the tumbling and the steady regimes we find a regime of shear rate in which there is a wagging of the direction of average molecular orientation. Finally, we show that shear-induced transitions from the isotropic to the nematic state are not expected to occur for lyotropic systems unless the biphasic concentration regime can be made narrower than that predicted by the Onsager theory.

## I. Introduction

One of the most distinctive phenomena observed in the flow of lyotropic liquid crystal polymers in the nematic or cholesteric state is that of negative steady-state first normal stress differences in shearing flow over a range of shear rate and concentration. For fluids that are isotropic at rest, the first normal stress difference ($N_1$) is zero or positive over all rates of shear, which means that the two surfaces between which the material is sheared tend to be pushed apart. However, in a pattern first seen 12 years ago by Kiss and Porter[1] in nematic poly($\gamma$-benzyl glutamate) solutions and reproduced since in other liquid crystalline solutions,[2-4] positive values of $N_1$ are found at low and high shear rates, with *negative* values occurring at intermediate shear rates.

This behavior remained an enigma until the recent theoretical work of Marrucci and Maffettone,[5] which for the first time clearly linked these normal stress transitions to a tendency of the direction of average molecular orientation to tumble in the shearing flow about the vorticity axis and to the arrest of the tumbling that eventually occurs as the shear rate is increased. In their calculations, Marrucci and Maffettone used the Doi theory to describe the dynamics of nematic liquid crystal polymers.[6] In earlier work with this theory, a closure approximation was used that artificially suppressed the tumbling tendency, and so only positive values of $N_1$ were predicted. Marrucci and Maffettone avoided closure approximations and yet kept the calculations simple by solving a two-dimensional version of the Doi theory. Thus the molecules were assumed to lie in a plane perpendicular to the vorticity axis—that is, in the plane parallel to both the direction of the velocity and the direction of the velocity gradient. Despite this rather gross simplification, the predicted range of shear rates over which $N_1$ is negative and the dependence of this range on polymer concentration are in excellent qualitative agreement with observations.

The purposes of this work are to confirm the basic conclusions of Marrucci and Maffettone, to remove some of the approximations of their work, and to extend their results by examining in more detail the process by which tumbling is arrested. Our approach differs from that of Marrucci and Maffettone in two significant ways. First, we consider the problem in three dimensions; that is we allow molecular orientation in the vorticity direction. Second, we use the Onsager[7] potential (described below) rather than that of Maier and Saupe[8] to model the excluded-volume interactions between rodlike molecules. Because Onsager rigorously derived his potential from a virial expansion, it becomes exact at low volume fractions of perfectly rigid rodlike molecules. Lyotropic solutions dilute enough for the Onsager theory to be accurate can be nematic if the polymer aspect ratio is very high (>100). The Maier–Saupe potential, on the other hand, has been rationalized either empirically or as a truncation of the Onsager potential[6] and is thus less likely to give quantitative predictions. Another advantage of the Onsager potential over that of Maier and Saupe is that the former gives a clear-cut prediction of the range of concentrations over which equilibrium nematic and isotropic phases can coexist and thus is well suited to the study of the influence of flow on the isotropic-to-nematic transition.[9-12]

To solve for the time-dependent orientation-distribution function, we make use of a newly developed algorithm that solves the Doi equation with the help of a set of orthogonal basis functions—the spherical harmonic functions. These functions allow accurate and economical representation of the orientation-distribution function and, indeed, Doi and Edwards have already used them to obtain this function in the presence of flow for rodlike molecules in solutions dilute enough that excluded-volume effects could be neglected altogether.[13]

In the following, we present Doi's evolution equation for the orientation-distribution function in the presence of flow, outline the numerical solution technique, and discuss the results. We shall also discuss a closure approximation that improves on that of Doi in that it predicts tumbling.

## II. The Doi Equation

We define $\psi(\mathbf{u})$ to be the probability that a thin perfectly rigid rodlike molecule has orientation parallel to the unit vector $\mathbf{u}$. The evolution of this distribution function in the presence of flow and excluded-volume effects was given by Doi:[6]

$$\frac{\partial \psi}{\partial t} + \frac{\partial}{\partial \mathbf{u}}\cdot[(\mathbf{u}\cdot\nabla\mathbf{v} - \mathbf{uuu}:\nabla\mathbf{v})\psi] = \bar{D}_r\frac{\partial}{\partial \mathbf{u}}\cdot\left[\frac{\partial \psi}{\partial \mathbf{u}} + \psi\frac{\partial}{\partial \mathbf{u}}\left(\frac{V_{ev}}{kT}\right)\right] = 0 \quad (1)$$

where $\nabla\mathbf{v}$ is the velocity gradient, $\bar{D}_r$ is an effective

0024-9297/90/2223-3983$02.50/0 

orientation-independent rotary diffusivity, $\partial/\partial\mathbf{u}$ is the gradient operator on the unit sphere, and $V_{ev}$ is an effective excluded-volume potential. Here we shall use the excluded-volume potential of Onsager:

$$V_{ev}(\mathbf{u}) = V_0(\mathbf{u}) = UkT\int \psi(\mathbf{u}') \sin(\mathbf{u}',\mathbf{u})\, d^2u' \quad (2)$$

In the above sin $(\mathbf{u}',\mathbf{u})$ is the sine of the angle between the unit vectors $\mathbf{u}'$ and $\mathbf{u}$ describing the orientations of two rods. The integral is over the surface of a unit sphere in orientation space. $U$ is a dimensionless concentration

$$U \equiv 2cdL^2 \quad (3)$$

where $d$ is the rod diameter, $L$ is its length, and $c$ is the number of molecules per unit volume.

Except in the dilute concentration regime, the rotary motion of each thin molecule is hindered by the presence of surrounding molecules. An approximate theory for the rotary Brownian diffusivity in concentration regimes where such hindering is strong was given by Doi and Edwards. This theory yields an expression for the orientation-dependent rotary diffusivity $\hat{D}_r$:

$$\hat{D}_r(\mathbf{u}) = D_r\left[\frac{4}{\pi}\int \sin(\mathbf{u},\mathbf{u}')\psi(\mathbf{u}')\, d^2u'\right]^{-2} \quad (4)$$

Here $D_r$ is the rotary diffusivity predicted for a rod in an isotropic solution of like rods from the theory of Doi and Edwards for semidilute solutions. This theory gives $D_r = \beta D_{r0}(cL^3)^{-2}$, where $D_{r0}$ is the rotary diffusivity for the rod in dilute solution and $\beta$ is an empirical coefficient[14] whose value has been found to be roughly $10^3$. In a matrix of oriented rods, the rotary diffusivity $\hat{D}_r$ of a rod depends on the orientation of that rod relative to that of the matrix rods, as expressed in eq 4. This dependence greatly complicates the theory. Following Doi and Edwards, we therefore replace $\hat{D}_r(\mathbf{u})$ with an averaged quantity $\bar{D}_r$:

$$1/\bar{D}_r = \langle \hat{D}_r^{-1/2}\rangle^2 = D_r^{-1}(4/\pi)^2[\int \psi(\mathbf{u})\psi(\mathbf{u}') \sin(\mathbf{u},\mathbf{u}')\, d^2u\, d^2u']^2 \quad (5)$$

Here $\langle ... \rangle$ denotes the average over the distribution function

$$\langle ... \rangle \equiv \int \psi(\mathbf{u}) ...\, d^2u$$

Although the averaging of $\hat{D}_r$ removes its dependence on $\mathbf{u}$, a dependence on the average degree of molecular orientation is retained. The higher the degree of orientation, the less the molecules hinder each other's rotary motion and the higher $\bar{D}_r$ becomes.

Once $\psi$ is computed from eq 1, the birefringence tensor and the stress tensor can be obtained. The birefringence tensor is proportional to $c\mathbf{S}$, where $\mathbf{S}$ is the *order parameter tensor*

$$\mathbf{S} \equiv \langle \mathbf{uu} - {}^1/_3\delta \rangle \quad (6)$$

Here $\delta$ is the unit tensor. The stress tensor is given by

$$\sigma = 3ckT\mathbf{S} + c\int \psi\left(\frac{\partial}{\partial\mathbf{u}}V_0\right)\mathbf{u}\, d^2u \quad (7)$$

This expression for the stress tensor neglects purely viscous terms, which we believe are small in regimes of concentration and shear rate that include those of interest here. If, however, the combined effects of shear and excluded volume make the scalar order parameter very high—say, as high as 0.9—then one can estimate that the viscous stress would contribute about 10% of the total stress for a typical molecular aspect ratio $(L/d)$ of 100. In the results presented here, $S$ remains below 0.9, and so we neglect the viscous terms. The viscous terms are included in the analysis of Marrucci and Maffettone.[5]

## III. The Numerical Technique

To solve eq 1, we follow Doi and Edwards[11] and expand $\psi(\mathbf{u})$ in a series of spherical harmonic functions $Y_l^m$:

$$\psi(\mathbf{u},t) = \sum_{\substack{l'=0\\ l' \text{ even}}}^{\infty}\sum_{m'=0}^{l'} b_{l'm'}|l'm') \quad (8)$$

where

$$|l'm') \equiv Y_{l'}^{m'}(\mathbf{u}) \quad \text{for } m' = 0 \quad (9a)$$

$$\equiv \frac{1}{2^{1/2}}(Y_{l'}^{m'}(\mathbf{u}) + (-1)^{m'}Y_{l'}^{-m'}(\mathbf{u})) \quad \text{for } m' \neq 0 \quad (9b)$$

We substitute this expression for $\psi(\mathbf{u})$ into eq 1, with $V_{ev}$ given by the Onsager formula (2), multiply the resulting equation by $|lm)$, and integrate over the unit sphere to give

$$\frac{\partial}{\partial t}(lm|\psi) = -\left(lm\left|\frac{\partial}{\partial\mathbf{u}}\cdot\{[\mathbf{u}\cdot\nabla\mathbf{v} - \mathbf{uuu}:\nabla\mathbf{v}]\psi\}\right.\right) + \bar{D}_r\left(lm\left|\frac{\partial}{\partial\mathbf{u}}\cdot\frac{\partial}{\partial\mathbf{u}}\psi\right.\right) + \frac{\bar{D}_r}{kT}\left(lm\left|\frac{\partial}{\partial\mathbf{u}}\cdot\left[\psi\frac{\partial}{\partial\mathbf{u}}V_{ev}\right]\right.\right) \quad (10)$$

In the above, we have defined

$$(lm|...) \equiv \int |lm) ...\, d^2u$$

where $(lm|...)$ is an inner product, since $|lm)$ is its own Hermitian conjugate; i.e., $(lm| = |lm)$ with $(lm|$ being the Hermitian conjugate of $|lm)$. We now replace the expressions enclosed within the symbols "| )" by their expansions in terms of spherical harmonic functions. The term on the left side and the second term on the right side of eq 10 can be written as integrals over the unit sphere of products of two spherical harmonic functions; these can be evaluated by using the orthonormality of these functions to give

$$\frac{\partial}{\partial t}b_{lm} = -\left(lm\left|\frac{\partial}{\partial\mathbf{u}}\cdot\{[\mathbf{u}\cdot\nabla\mathbf{v} - \mathbf{uuu}:\nabla\mathbf{v}]\psi\}\right.\right) + 6\bar{D}_r l(l+1)b_{lm} + \frac{\bar{D}_r}{kT}\left(lm\left|\frac{\partial}{\partial\mathbf{u}}\cdot\left[\psi\frac{\partial}{\partial\mathbf{u}}V_{ev}\right]\right.\right) \quad (11)$$

The remaining convection and excluded-volume terms can be reduced to integrals over $d^2u$ of products of three spherical harmonic functions $Y_l^m Y_{l'}^{m'} Y_{l''}^{m''}$. These can be evaluated by using formulas developed for quantum mechanical calculations. The resulting expressions are complicated functions of the $b_{lm}$'s described elsewhere.[15] The formula for the stress tensor in eq 7 can also be reduced to an expression involving only the $b_{lm}$'s, as is shown elsewhere. The expression for $\bar{D}_r$ was given by Doi and Edwards[13]

$$\bar{D}_r = D_r\left(1 - 8\pi\sum_{\substack{l=2\\ l \text{ even}}}^{\infty}\sum_{m=0}^{l}\left(\frac{l-1}{l+2}\right)\left[\frac{(l-3)!!}{l!!}\right]^2 b_{lm}{}^2\right)^{-2} \quad (12)$$

We solve eq 11 by numerical integration using a fourth-order Runge–Kutta technique. Summations, such as that in eq 8, are truncated at a finite value of $l$ that we denote by $l_{max}$.

## IV. Results for Isotropic Phases

In the Onsager theory, when $U \leq U_1 = 8.38$, the equilibrium phase is isotropic—that is, $S^{eq} = 0$, where $S$ is the *scalar order parameter* defined by

$$S \equiv ({}^3/_2\mathbf{S}:\mathbf{S})^{1/2} \quad (13)$$

$S$ lies in the range 0–1, with $S = 0$ for a completely isotropic

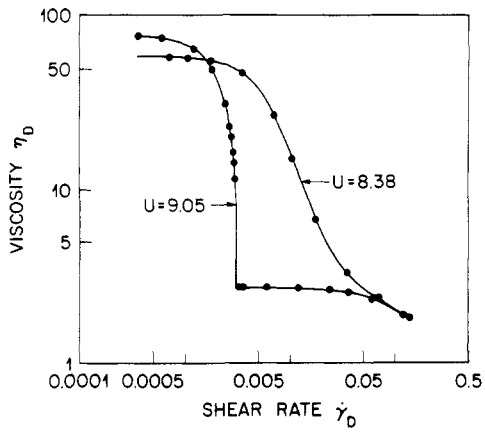


**Figure 1.** Steady-state shear viscosity $\eta_D$ versus shear rate $\dot{\gamma}_D$ for dimensionless concentrations $U$ of 8.38 and 9.05. For these calculations, $l_{max} = 12$.

distribution of orientations and $S = 1$ for rods that are all aligned in the same direction. When $U \geq U_2 = 10.67$, the equilibrium phase is nematic, and $S^{eq} > 0$. If $U_1 < U < U_2$, the solution at equilibrium is biphasic; the concentrations of the coexisting phases are such that $U = U_1 = 8.38$ for the isotropic phase while $U = U_2 = 10.67$ for the anisotropic phase. A metastable isotropic solution can exist for $U > 8.38$, but when $U \geq U^* = 10.19$, this solution is absolutely unstable to formation of nematic order. Metastable nematic order exists for concentrations somewhat below $U^*$, and hence there is range of values of $U$ below $U^*$ for which there are at least two metastable phases, one nematic and the other isotropic. The lowest value of $U$ for which an absolutely stable nematic single phase can exist is $U = 10.67$.

To obtain the predicted shear-flow properties of phases that are isotropic at rest, we compute the time evolution of the $b_{lm}$'s under a steady shearing flow that starts at $t = 0$. We set the initial values of all the $b_{lm}$'s to zero except $b_{00}$, which is set to $1/(4\pi)^{1/2}$; this corresponds to an isotropic orientation distribution. We then integrate eq 11 as described in section III, until steady-state values of the $b_{lm}$'s are obtained. From these, the stresses are calculated from eq 7, as discussed elsewhere.[15] To compare viscoelastic properties at different values of $U$ with corresponding experiments, we shall suppose that $U$ is varied by changing the concentration of polymer $c$, holding the molecular weight fixed. Since $U \propto c$, the rotational diffusivity $D_r$ is proportional to $U^{-2}$ according to the Doi theory. Defining the dimensionless shear rate $\Gamma$ by $\Gamma \equiv \dot{\gamma}/D_r$, the concentration dependence of the *dimensional* shear rate is proportional to $U^{-2}\Gamma \equiv \dot{\gamma}_D$. Also the concentration dependence of the product of the dimensionless stress $\sigma/ckT$ and $U$ is proportional to that of the dimensional stress. The concentration dependence of the dimensional viscosity is thus proportional to $U^3\sigma_{xz}/\Gamma ckT \equiv \eta_D$, where we take $x$ as the flow direction and $z$ as the direction parallel to the velocity gradient.

Figure 1 plots the steady-state shear velocity $\eta_D$ against the shear rate $\dot{\gamma}_D$ for $U = 8.38$ and $U = 9.05$. As noted earlier, $U = 8.38$ is the highest value of $U$ for which there is an absolutely stable equilibrium isotropic phase. At $U = 9.05$, there are two metastable phases, one isotropic and the other nematic. Note in Figure 1 that for $U = 9.05$ there is a discontinuous drop in $\eta_D$ as $\dot{\gamma}_D$ is raised above 0.003. For shear rates $\dot{\gamma}_D$ between 0.003 and about 0.02, the steady-state shear viscosity is nearly constant, and its value is equal to the zero-shear viscosity of the metastable nematic phase. Furthermore, the first normal stress difference in this range of shear rates is *negative*, which is also a characteristic of the nematic state. But most significantly, if the shearing flow with $\dot{\gamma}_D \geq 0.003$ ceases after steady state is reached, the orientation-distribution function relaxes to the static nematic solution of eq 11 rather than to the static isotropic solution that was the starting state at the inception of shearing. Thus we can say for $U = 9.05$ that a critical rate of shearing induces a transition to an anisotropic phase. When shearing ceases for $U = 8.38$, the distribution function relaxes back to an isotropic solution for all values of $\dot{\gamma}_D$. Thus for $U = 8.38$, shearing cannot induce a transition to a liquid crystalline state.

The concentration $U = 9.05$ is relatively close to the stability limit for the isotropic phase; i.e., $(U^* - 9.05)/U^* = 1/9$. Mead and Larson[11] have shown that the Doi theory with the Doi closure approximation and the Maier–Saupe potential also shows a shear-induced discontinuous phase transition for values of $U$ large enough that $(U^* - U)/U^* \lesssim 1/6$. For smaller values of $U$, the steady-state value of $\eta_D$ was found to be a continuous function of $\dot{\gamma}_D$. For a lyotropic system, that is, a system in which the nematic state is induced by changes in polymer concentration rather than temperature, the Maier–Saupe potential is unable to predict the maximum value of $U$ for which an absolutely stable equilibrium isotropic phase exists, and thus the Maier–Saupe potential does not allow one to assess whether or not discontinuous shear-induced phase transitions are likely to be seen. The Onsager potential, however, predicts that $U = 8.38$ is the maximum value of $U$ for which there is an absolutely stable isotropic equilibrium phase. For this value of $U$, $(U^* - U)/U^* = 1/5.6$, which according to Figure 1 is too far from the stability limit of the isotropic phase for a discontinuous shear-induced phase transition to occur. This prediction is consistent with experimental work in lyotropic systems, which have so far failed to show any discontinuous changes in steady-state shear viscosity as a function of shear rate.[1,11] Since our calculations assume a homogeneous state of matter, we are here overlooking the possibility that a transition might be produced by a coupling of the shear flow to concentration fluctuations. Besides the possibility that fluctuation effects might induce a transition in shearing flows of ideal lyotropic systems, there also remain the possibilities of finding flow-induced transitions in nonshearing flows,[9,10,12] in shearing flows of lyotropic systems for which nonidealities make the gap between $U_1$ and $U^*$ narrower than that predicted by the Onsager theory, and in thermotropic systems—i.e., solvent-free systems in which the nematic state is brought about by changes in temperature.

## V. Results for Anisotropic Phases

**A. Equilibrium.** For a shearing flow with $x$ the flow direction, $z$ the gradient direction, and $y$ the vorticity direction, the nonzero components of $\mathbf{S}$ are related to the coefficients $b_{lm}$ by[13]

$$S_{xz} = -(4\pi/15)^{1/2}b_{21} \tag{14a}$$

$$S_{xx} - S_{zz} = (4\pi/15)^{1/2}(b_{22} - 3^{1/2}b_{20}) \tag{14b}$$

$$S_{zz} - S_{yy} = (4\pi/15)^{1/2}(b_{22} + 3^{1/2}b_{20}) \tag{14c}$$

At thermodynamic equilibrium in the absence of flow, the scalar order parameter $S$—defined by eq 13—takes on a value, $S^{eq}$, that depends only on the parameter $U$, and $\mathbf{S}$ has uniaxial symmetry; that is

$$\mathbf{S} = S^{eq}(\mathbf{nn} - {}^1/_3\delta) \tag{15}$$

where the unit vector $\mathbf{n}$ is called the director. We compute the equilibrium distribution function $\psi^{eq}$ at $U = 10.67$ and

$U = 12$ by starting from an isotropic state where $b_{00} = 1/(4\pi)^{1/2}$ and all other $b_{lm}$'s = 0. We then perturb $b_{20}$ in the positive direction and solve eq 11 by Runge–Kutta integration until the $b_{lm}$'s reach constant equilibrium values. In the absence of any field, the equilibrium state is degenerate with respect to the director **n**; so the initial perturbation determines **n**. For the perturbation chosen here the director points in the $z$ direction; that is, $n_x = 0$, $n_y = 0$, and $n_z = 1$. From the computer equilibrium $b_{lm}$'s, we obtain $S^{eq}$ from (13) and (14). The values of $S^{eq}$ we obtain for various values of $l_{max}$ are tabulated below.

| $l_{max}$ | $S^{eq}$ ($U = 10.67$) | $S^{eq}$ ($U = 12$) |
|---|---|---|
| 4 | 0.606 | 0.608 |
| 8 | 0.787 | 0.840 |
| 12 | 0.792 | 0.856 |
| 16 | 0.792 | 0.856 |

Thus $S^{eq}$ converges, to 0.792 for $U = 10.67$ and to 0.856 for $U = 12$, when $l_{max} \geq 12$. The value for $U = 10.67$ agrees with that obtained by Lekkerkerker et al.[16]

**B. Low Rates of Shear: Tumbling.** Under a weak shearing field, the scalar order parameter $S$ is not significantly perturbed from its equilibrium value, but the director **n** can rotate during the shearing. The order parameter tensor is then given by

$$\mathbf{S} = S^{eq}[\mathbf{n}(t)\mathbf{n}(t) - {}^1/_3\delta] \tag{16}$$

Hence the evolution of the order parameter tensor in this limit is determined by the time evolution of **n**, which is obtained from the Leslie–Ericksen limit of the Doi theory:

$$\frac{\partial}{\partial t}\mathbf{n} = \omega^T\cdot\mathbf{n} + \lambda(\mathbf{D}\cdot\mathbf{n} - \mathbf{D}:\mathbf{nnn}) \tag{17}$$

**D** and $\omega$ are respectively the straining and vorticity tensors

$$\mathbf{D} \equiv {}^1/_2(\nabla\mathbf{v} + \nabla\mathbf{v}^T) \tag{18a}$$

$$\omega \equiv {}^1/_2(\nabla\mathbf{v} - \nabla\mathbf{v}^T) \tag{18b}$$

and the superscript "T" denotes the transpose. The parameter $\lambda$ depends on the equilibrium distribution function $\psi^{eq}$ and therefore on $U$. When $\lambda > 1$, the straining motion dominates and **n** tends toward a steady-state orientation angle $\theta$ with respect to the flow direction, where

$$\tan\theta = \left[\frac{\lambda - 1}{\lambda + 1}\right]^{1/2} \tag{19}$$

When $\lambda < 1$, vorticity dominates over straining and the director can find no steady-state orientation; it then *tumbles* continuously. The period $P$ required for the director to rotate through an angle of $2\pi$ is

$$P = 4\pi/[\dot\gamma(1 - \lambda^2)^{1/2}] \tag{20}$$

where $\dot\gamma$ is the shear rate.

To calculate $\lambda$ from the Doi theory, we multiply eq 1 by $(\mathbf{uu} - {}^1/_3\delta)$ and integrate the resulting equation over the equilibrium distribution function $\psi^{eq}$. At low shear rates, the Brownian and excluded-volume terms cancel each other and the remaining terms give

$$\frac{\partial}{\partial t}\mathbf{S} = {}^2/_3\mathbf{D} + \omega^T\cdot\mathbf{S} + \mathbf{S}\cdot\omega + \mathbf{D}\cdot\mathbf{S} + \mathbf{S}\cdot\mathbf{D} - 2\mathbf{D}:\langle\mathbf{uuuu}\rangle \tag{21}$$

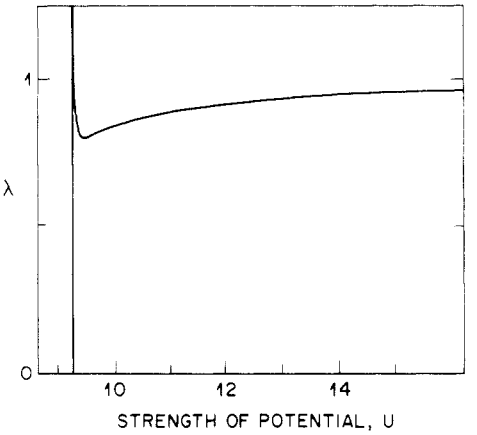


**Figure 2.** Tumbling parameter $\lambda$ as a function of dimensionless concentration $U$ calculated from the Doi theory with the Onsager potential (from Kuzuu and Doi[17]).

Dotting this equation with **n** and using eq 16 for **S** give

$$S^{eq}\frac{\partial}{\partial t}\mathbf{n} = S^{eq}\omega^T\cdot\mathbf{n} + {}^2/_3\mathbf{D}\cdot\mathbf{n} + {}^1/_3S^{eq}\mathbf{D}\cdot\mathbf{n} - 2\mathbf{D}:\langle\mathbf{uuuu}\rangle\cdot\mathbf{n} + \text{terms parallel to } \mathbf{n} \tag{22}$$

The terms parallel to **n** serve only to keep the magnitude of **n** fixed at unity and are not important in determining $\lambda$.

To proceed, the term $\mathbf{D}:\langle\mathbf{uuuu}\rangle$ must be reduced to an expression involving only **D**, **n**, and $U$. The most accurate way to do this is to first obtain $\psi^{eq}$ and then evaluate $\langle\mathbf{uuuu}\rangle$. Kuzuu and Doi[17] did this using the Onsager potential to determine $\psi^{eq}$ and found the result replotted in Figure 2. Note that if $U$ is less than 9.2 or so, $\lambda$ is large and there is no tumbling. As $U$ increases, $\lambda$ at first decreases, passes through unity at $U \approx 9.3$, then goes through a minimum, and increases toward unity as $U \to \infty$. The maximum tendency to tumble (i.e., the minimum value of $\lambda$) occurs at an intermediate value of $U$, with the tumbling tendency disappearing both at small $U$ and in the limit of very large $U$. When $U$ is very large, $S^{eq} \to 1$; i.e., the molecules become perfectly aligned. Rigid molecules of very high aspect ratio in a shearing flow experience a torque at any orientation except when they are parallel to $x$, the flow direction. Thus for $S^{eq} = 1$, shearing rotates the molecules until they are parallel to the flow direction and at this orientation they cease to rotate. If $S^{eq}$ is slightly less than unity, however, molecules deviate slightly from the average orientation, and even when the average orientation is parallel to the $x$ axis, there is a torque on molecules that are not exactly parallel to $x$. Because of the excluded-volume potential, the torque on any one molecule is transmitted to the others and the whole assembly of molecules continues rotating even at the instant the average direction is parallel to $x$. When $S^{eq}$ is small, it is evident from eq 22 that the rotation of the director is dominated by the straining motion that tends to orient the director parallel to the direction of maximum straining, and there is no tumbling. Thus the rate of tumbling of the director is maximized, and the value of $\lambda$ is minimized, at an intermediate value of $S^{eq}$. Note, however, that at any concentration at which the nematic phase is absolutely stable (that is, for which $U \geq 10.67$), tumbling is predicted.

It is of interest to try to approximate $\mathbf{D}:\langle\mathbf{uuuu}\rangle$ by an analytic expression involving only **D** and $\langle\mathbf{uu}\rangle$. Such an expression not only makes evaluation of $\lambda$ trivial but would also be of use in obtaining simplified approximate solutions of eq 1 for moderate and large shear rates. The simplest

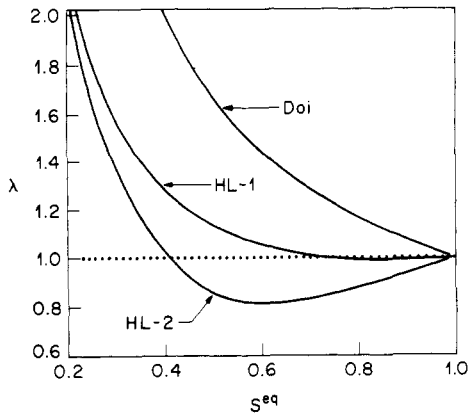


**Figure 3.** Tumbling parameter λ as a function of the equilibrium order parameter $S^{eq}$ calculated using the Doi closure approximation (eq 23) and those of Hinch and Leal (eq 25 for HL-1 and eq 26 for HL-2).

approximate expression is that proposed by Doi:

$$\mathbf{D}:\langle\mathbf{uuuu}\rangle \approx \mathbf{D}:\langle\mathbf{uu}\rangle\langle\mathbf{uu}\rangle \tag{23}$$

This approximation becomes exact as $S^{eq}$ approaches unity, that is, as the rods approach perfect alignment with each other. Using $\langle\mathbf{uu}\rangle = S^{eq}(\mathbf{nn} - {}^1/_3\delta)$, we find that with the approximation in eq 23, $\mathbf{D}:\langle\mathbf{uuuu}\rangle\cdot\mathbf{n}$ is parallel to $\mathbf{n}$. Thus, within this approximation, eq 22 gives

$$\frac{\partial}{\partial t}\mathbf{n} = \omega^{T}\cdot\mathbf{n} + \frac{1}{3S^{eq}}(2 + S^{eq})\mathbf{D}\cdot\mathbf{n} + \text{terms parallel to } \mathbf{n} \tag{24}$$

Comparing this to eq 17, we find that $\lambda = (2 + S^{eq})/3S^{eq}$, which is greater than unity for all $S^{eq} < 1$. Hence, the director does not tumble but tends toward a stable angle $\phi$, which approaches zero as $U$ becomes large and $S^{eq}$ approaches unity. Thus as shown in Figure 3, the correct asymptote $\lambda \to 1$ is obtained at large $U$, but it is approached from the wrong direction, that is, from above rather than below, and consequently the approximation fails to predict tumbling.

More accurate approximate expressions were suggested by Hinch and Leal.[18] The first of these is

$$\mathbf{D}:\langle\mathbf{uuuu}\rangle \approx \frac{1}{5}\{6\langle\mathbf{uu}\rangle\cdot\mathbf{D}\cdot\langle\mathbf{uu}\rangle - \langle\mathbf{uu}\rangle\langle\mathbf{uu}\rangle:\mathbf{D} - 2\delta(\langle\mathbf{uu}\rangle\cdot\langle\mathbf{uu}\rangle):\mathbf{D} + 2\delta\langle\mathbf{uu}\rangle:\mathbf{D}\} \tag{25}$$

and the second (still more accurate expression) is

$$\mathbf{D}:\langle\mathbf{uuuu}\rangle \approx \langle\mathbf{uu}\rangle\langle\mathbf{uu}\rangle:\mathbf{D} + 2[\langle\mathbf{uu}\rangle\cdot\mathbf{D}\cdot\langle\mathbf{uu}\rangle - \langle\mathbf{uu}\rangle^2\langle\mathbf{uu}\rangle^2:\mathbf{D}/(\delta:\langle\mathbf{uu}\rangle^2)] + \alpha\left[\frac{52}{315}\mathbf{D} - \frac{8}{21}\left(\mathbf{D}\cdot\langle\mathbf{uu}\rangle + \langle\mathbf{uu}\rangle\cdot\mathbf{D} - \frac{2}{3}\delta\langle\mathbf{uu}\rangle:\mathbf{D}\right)\right] \tag{26a}$$

with

$$\alpha \equiv \exp[2(1 - 3\langle\mathbf{uu}\rangle^2:\delta)/(1 - \langle\mathbf{uu}\rangle^2:\delta)] \tag{26b}$$

These expressions become exact not only in the limit $S^{eq} \to 1$ but also when $S^{eq}$ becomes small. From (25) we obtain

$$\lambda = \frac{6 + S^{eq} + 8(S^{eq})^2}{15S^{eq}} \tag{27}$$

while eq 26 gives

$$\lambda = \frac{1}{9S^{eq}}\left\{2 - S^{eq} + 8(S^{eq})^2 + \frac{56 + 80S^{eq}}{35}\exp[-6(S^{eq})^2/(1 - (S^{eq})^2)]\right\} \tag{28}$$

These expressions, plotted in Figure 3, are in qualitative agreement with those of Kuzuu and Doi; that is, as $U$ and therefore $S^{eq}$ increases, λ at first decreases and passes through unity; thereafter λ reaches a minimum and then increases toward unity as $S^{eq} \to 1$. Thus, for the first Hinch–Leal approximation, tumbling is predicted for $S^{eq} > 0.75$, while for the second (better) approximation, it is predicted for $S^{eq} > 0.4$. The minimum value of λ within the first Hinch–Leal closure approximation is 0.98, which is very close to unity, while within the second approximation it is 0.81, much closer to the minimum value of about 0.8 obtained by Kuzuu and Doi. Thus the Hinch–Leal closure approximations lead to predictions of tumbling when $S^{eq}$ is well above zero but less than unity.

Tumbling can also occur in small-molecule nematics when the temperature is close to that for a transition to smectic order.[19] For a monodomain small-molecule nematic in the gap between parallel plates with uniform and strongly anchored molecular orientation at the plate–liquid interface, tumbling in the bulk during shearing of the sample could theoretically be halted once the gradients in molecular orientation that build up between the interface and the bulk produce torques large enough to balance the viscous torques that produce tumbling.[20] For polymeric nematics, however, viscous torques are typically at least 2 orders of magnitude larger than those prevalent in flow of small-molecule nematics, and under most conditions it is unlikely that gradient stresses (or Frank stresses[21]) that build up at the interface would propagate far enough into the bulk to halt tumbling. Defects or inhomogeneities typically present in polymeric liquid crystals, however, do produce significant Frank stresses; their influence on tumbling is uncertain.

**C. Moderate Rates of Shear: A Transition from Tumbling to Wagging.** As the shear rate is increased the distribution function begins to distort, and $S$ deviates increasingly from $S^{eq}$. This regime of moderate shear rates is characterized by $\Gamma \equiv \dot{\gamma}/D_r$ in the range 1–30 or so.

The algorithm outlined in section III is an accurate means of computing the predictions of the Doi theory with the Onsager potential for shear rates in this regime. In the calculations described here, the distribution function $\psi$, the order parameter tensor $\mathbf{S}$ (which is proportional to the birefringence), and the stress tensor $\sigma$ are computed as functions of time following start-up of steady shearing. Calculations with both $l_{max} = 12$ and $l_{max} = 16$ were carried out. For $\Gamma \leq 25$, the results for these two values of $l_{max}$ are almost identical, while for $\Gamma > 25$ modest differences are found, especially in the first normal stress difference; these differences grow to at most 25% as Γ increased to 400. Thus calculations for $l_{max} = 12$ are limited to the regime $\Gamma \leq 25$; for higher values of Γ, we take $l_{max} = 16$.

At the start of steady shearing the distribution function is taken to be at equilibrium with the director $\mathbf{n}$ initially pointing in the $z$ direction, that is, the direction of the gradient in velocity. Here the dimensionless concentration $U$ is set equal to 10.67, which is the lowest value for which a nematic phase is obtained at equilibrium. Thus the initial order parameter tensor is given by eq 15 with $S^{eq} = 0.792$ and $\mathbf{n} = (n_x,n_y,n_z) = (0,0,1)$. Once shearing begins in this regime of shear rates, the scalar order parameter departs significantly from $S^{eq}$ and the tensor order parameter is no longer uniaxial and so cannot be represented by eq 16. Thus the director can no longer be defined. The order parameter tensor remains symmetric, however, and thus has three mutually perpendicular principal axes. Because of the flow symmetry, one of these axes points along the $y$ axis, and the other two lie in the $x$–$z$ plane. Since these latter two are mutually

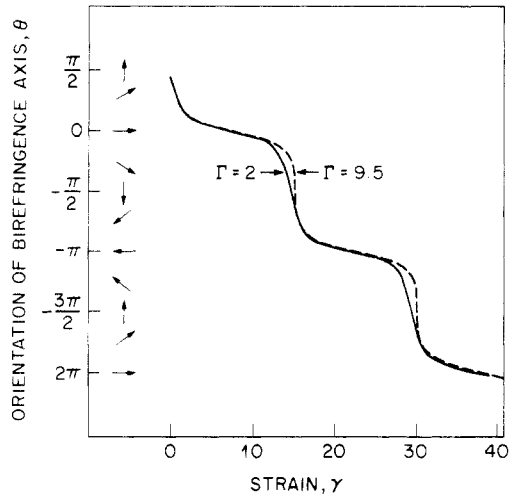


**Figure 4.** Orientation of the birefringence axis $\theta$ as a function of shear strain $\gamma$ for dimensionless shear rates $\Gamma$ of 2 and 9.5. In Figures 4–15, $U = 10.67$.

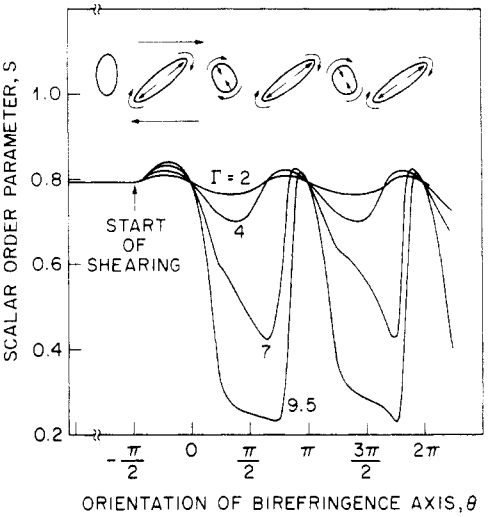


**Figure 5.** Scalar order parameter $S$ as a function of shear strain $\gamma$ for dimensionless shear rates $\Gamma$ of 2, 4, 7, and 9.5.

perpendicular, the angle of orientation of one of them with respect to our coordinate system determines the orientation of the other. Thus the orientations of the three principal axes of the tensor **S** are determined by the orientation of just one of the two axes that lie in the $x$–$z$ plane. Before flow starts, one of these two axes is parallel to the director and hence parallel to the $z$ axis; we shall call this principal axis of **S** the birefringence axis. For weak shearing flows for which the director can be defined, the birefringence axis remains parallel to the director during flow. Thus the definition of the birefringence axis generalizes that of the director in that the two definitions are equivalent at low shear rates where the latter is defined, but unlike the latter the former is defined at any shear rate. We shall track the orientation of the birefringence axis as a function of time after initiation of shearing and define $\theta$ as the angle this axis makes with the flow direction; initially $\theta = \pi/2$. To within a multiple of $\pi/2$, $\theta$ is given by

$$\frac{S_{xz}}{S_{xx} - S_{zz}} = \frac{1}{2}\tan(2\theta) \tag{29}$$

While $\theta$ gives an average direction of molecular orientation, the scalar order parameter $S$—which is defined at any shear rate by eq 13—characterizes the instantaneous degree of orientation.

In Figure 4, $\theta$ is plotted as a function of strain $\gamma = \dot{\gamma}t$ following initiation of steady shearing at dimensionless shear rates of 2 and 9.5. At these modest shear rates the birefringence axis tumbles continuously. For $\Gamma = 2$, a period of 30.2 strain units is required for rotation through an angle of $2\pi$. From this period we find using eq 20 that $\lambda = 0.91$, in reasonable agreement with the calculation of Kuzuu and Doi, which gives $\lambda \approx 0.87$ for $U = 10.67$. This value of $\lambda$ is also in reasonable agreement with the value 0.87 obtained from the second Hinch–Leal approximation, i.e., eq 28 with $S^{eq} = 0.792$. As the birefringence axis tumbles in its orbit, $S$ oscillates around $S^{eq}$, with maximum departures from $S^{eq}$ of only about $\pm 2\%$ for $\Gamma = 2$; see Figure 5. The maximum positive departures occur at angles $\theta$ close to $\pi/4 - n\pi$, where $n$ is a nonnegative integer, and the maximum negative departures occur at $\theta$ close to $-\pi/4 - n\pi$. These angles correspond respectively to the extensional and compressional directions of the velocity gradient tensor in shearing flow. Stated more precisely, of the two nonzero eigenvectors of the symmetric part of the velocity gradient tensor, the one for which the eigenvalue is positive (corresponding to extension) is parallel to $\pi/4 - n\pi$, while the one whose eigenvalue is negative (corresponding to compression) is parallel to $-\pi/4 - n\pi$. Thus as the birefringence axis tumbles through orientations for which the kinematics correspond to extension and then to compression, the birefringence ellipse is alternately stretched and then compressed.

When $\Gamma$ increases from 2 to 9.5 (Figure 4), the period changes little, but the departures of the scalar order parameter $S$ from its equilibrium value $S^{eq}$ are greatly magnified (Figure 5), and the angles at which the departures are greatest shift in the negative direction. Thus as $\Gamma$ increases, the time at which $S$ is at its maximum departure from $S^{eq}$ lags more and more behind the time at which $\theta$ is at an orientation where the extension or compression is greatest. The lag occurs when the rate of tumbling of the birefringence axis is comparable to or faster than the rate at which the distribution function can relax. The deflection of $S$ from $S^{eq}$—especially the negative deflection—becomes larger as $\Gamma$ increases. At $\Gamma = 9.5$, $S$ at times becomes as low as 0.25, which is closer to that of a completely isotropic solution ($S = 0$) than to the equilibrium value of 0.792! The ellipses in Figure 5 give a pictorial representation of the evolution of the tensor order parameter **S** during tumbling. The orientation of the major axis of this ellipse illustrates the orientation of the birefringence axis—that is, the major axis of the tensor **S**—while the variations in the ellipse's eccentricity during the tumbling illustrate the corresponding variations in the scalar order parameter.

Figure 6 shows $\theta$ and $S$ as functions of strain at a slightly higher shear rate, $\Gamma = 10$. Note that tumbling has given way to an oscillation or *wagging* of the birefringence axis between angles of about $0.2\pi$ and $-0.2\pi$. During this wagging, as $\theta$ decreases toward $-0.2\pi$, the order parameter $S$ decreases, as we also saw at lower shear rates for which tumbling occurs. We noted earlier that for low shear rates where $S$ remains close to $S^{eq}$, the tendency of the birefringence axis or the director to tumble disappears when $S^{eq}$ drops below a critical value (due in that case to a reduction in $U$). One might therefore expect that the tumbling tendency could also be suppressed at $U = 10.67$ in those portions of the cycle of the birefringence axis in which $S$ is reduced sufficiently by shearing. This is indeed consistent with the behavior of the birefringence axis shown in Figure 6. Note in particular that the clockwise rotation of the birefringence axis abruptly ceases at $\theta \approx -0.20\pi$ when $S$ drops below about 0.5; the birefringence axis thereafter

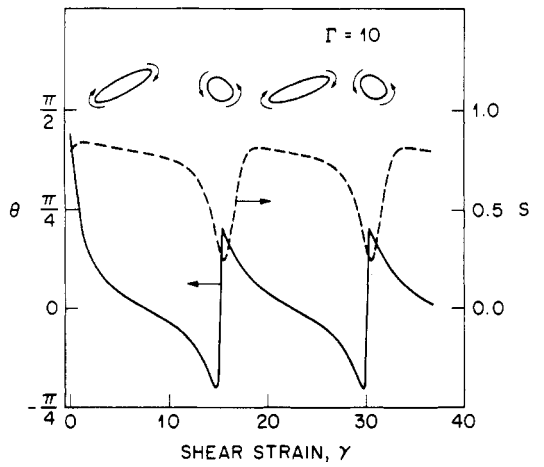


**Figure 6.** Orientation of the birefringence axis $\theta$ and order parameter $S$ as functions of shear strain $\gamma$ for a dimensionless shear rate $\Gamma$ of 10.

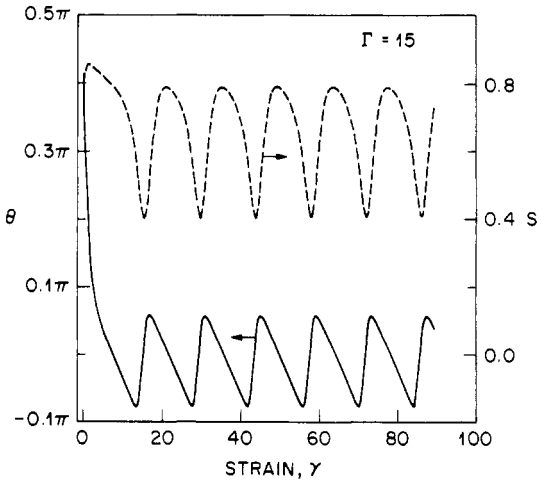


**Figure 7.** Orientation of the birefringence axis $\theta$ and order parameter $S$ as functions of shear strain $\gamma$ for a dimensionless shear rate $\Gamma$ of 15.

retreats for a time in the counterclockwise direction. When $\theta$ rises above 0 or so, most of the molecules are no longer oriented in directions in which the flow is compressional, and the order parameter $S$ thereafter begins to increase again. Eventually $S$ becomes large enough that the tumbling tendency is restored, and the birefringence axis can again rotate clockwise through the angle $\theta = 0$ and continue rotating clockwise until $S$ again drops enough and the cycle repeats itself. The above discussion is necessarily qualitative since the direction in which the birefringence axis tends to rotate depends not only on the instantaneous value of $S$ but also on the angle $\theta$ and on the instantaneous distribution function $\psi$.

When $\Gamma$ is raised to 15, the wagging persists, but its amplitude is diminished to $\pm 0.07\pi$; see Figure 7. The amplitude of the oscillation continues to decreases as $\Gamma$ increases.

**D. High Rates of Shear: Existence of a Steady State.** When $\Gamma$ reaches 25, the continuous wagging of the birefringence axis is replaced by a weakly damped oscillation that eventually leads to a slightly negative steady-state orientation angle (Figure 8). The damping increases monotonically as $\Gamma$ increases, so that for $\Gamma \geq 25$, steady-state values of $\theta$ and of the birefringence and stress tensors can be computed. The steady-state values of $\theta$ and $S$ increase slowly and monotonically as $\Gamma$ increases; see Figure 9. Note that $S$ exceeds its equilibrium value of 0.792 only when $\Gamma$ reaches 800.

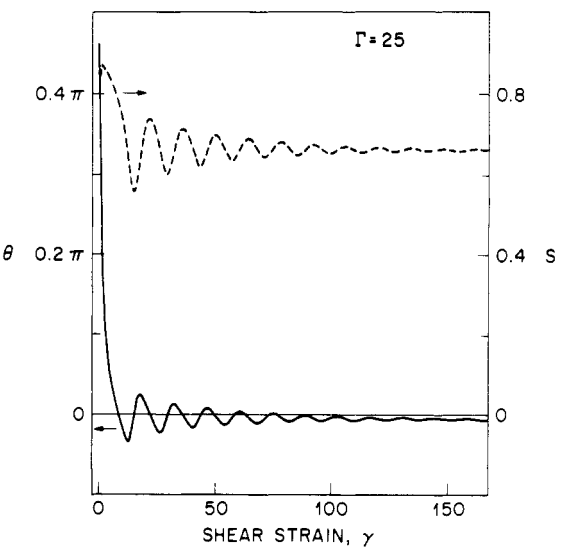


**Figure 8.** Orientation of the birefringence axis $\theta$ and order parameter $S$ as functions of shear strain $\gamma$ for a dimensionless shear rate $\Gamma$ of 25.

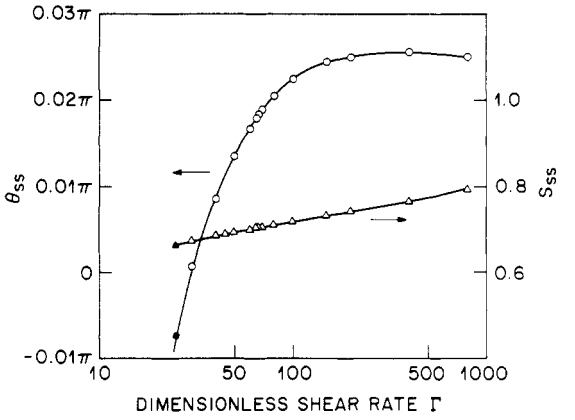


**Figure 9.** Steady-state values of the orientation of the birefringence axis $\theta$ and the order parameter $S$ as functions dimensionless shear rate $\Gamma$. The solid symbols represent calculations with $l_{max} = 12$, while $l_{max} = 16$ for the open symbols.

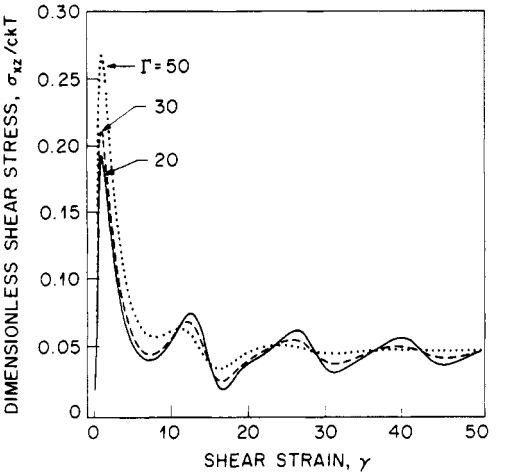


**Figure 10.** Dimensionless shear stress $\sigma_{xz}/ckT$ as a function of strain $\gamma$ for dimensionless shear rates $\Gamma$ of 20, 30, and 50.

The damped oscillations in $\theta$ are reflected in similar oscillations in stress and birefringence. Figure 10 shows the shear stress as a function of strain for $\Gamma = 20$, 30, and 50. The strains at which the stress peaks occur are roughly independent of $\Gamma$, while the damping of the oscillation increases with increasing $\Gamma$. Shear stress oscillations are frequently observed in start-up of shearing flows of liquid

crystalline polymers, and Mewis and Moldenaers[22] have also observed that the strains at which the shear stress goes through maxima are independent of shear rate.

## VI. Shear Stress and Normal Stress Differences as Functions of Shear Rate

For $\Gamma \geq 25$, steady-state shear and normal stresses can be computed, while for $\Gamma \leq 25$, there is no steady state. The existence of a critical shear rate above which steady-state solutions exist and below which there is no steady-state has been already noted in the two-dimensional calculations of Marrucci and Maffettone.[5] Experimentally, apparent steady-state values of the stresses are reported even at low shear rates. However, it has also been reported that values of the normal stresses are sometimes really averages over time of a signal that actually contains large oscillations in normal stress.[23] The range of shear rates over which these oscillations occur has apparently not yet been investigated, and so the relationship, if any, between these oscillations and those predicted by the Doi theory cannot be assessed. A further complication is that the samples studied experimentally have invariably been polydomain specimens—that is, at rest they contained many orientational defects so that the direction of molecular orientation was only uniform over micron-size regions called domains. In the theoretical work reported here, the evolution of the orientation distribution function is computed under the assumption that the initial orientation of the director is uniform and parallel to the $z$ axis. Since for $\Gamma \geq 25$, the distribution function theoretically tends toward a steady state that is expected to be independent of the initial orientation, the distribution function in any domain should approach that of any other domain after prolonged shearing, and the polydomain character of the real specimen might not significantly affect the steady-state measurements. Thus we believe that the theoretical steady-state results reported here can be meaningfully compared to steady-state experimental data. However, for $\Gamma \leq 25$, it is predicted that the orientation distribution never reaches a steady state; under these conditions it would seem that the polydomain character of the sample must influence the measured response.

The simplest way to account for the effect of polydomains is to average the response of a single domain to the imposed flow field over the distribution of domain orientations, the response of a single domain being obtained by treating it as though it were part of a homogeneous sample. This approach neglects the influence of gradient terms—i.e., the Frank elastic terms—on the evolution of the orientation-distribution function and on the stress. One must also decide whether to assume that the shear rate is the same in each domain and consequently the stress varies from domain to domain or to assume that the shear component of the stress tensor is the same in each domain and the shear rate varies from domain to domain.[24] In reality, of course, both the local stress tensor and the local flow field vary in an interrelated fashion so that the momentum balance equation is everywhere satisfied. In some transport problems in composite materials, however, it can be shown that the two alternatives above give respectively upper and lower bounds for the transport coefficients.[25] Here we choose to keep the shear rate constant and allow the stress to vary from domain to domain. It may be reasonable to assume that at long times after start-up of shearing each domain falls into a tumbling or wagging cycle that is identical, except for a phase shift, with that followed by any other domain. With these assumptions, the average stress tensor for the polydomain sample can be calculated by averaging the stress tensor for a single domain over one period of its cycle.

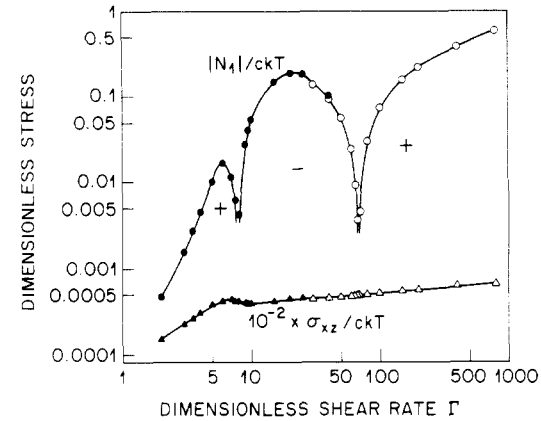


**Figure 11.** Dimensionless shear stress $\sigma_{xz}/ckT$ and first normal stress difference $N_1/ckT$ as functions of dimensionless shear rate $\Gamma$. The symbols are defined in the caption for Figure 9.

In Figure 11 the shear stress and first normal stress difference are plotted as functions of dimensionless shear rate $\Gamma$ for $U = 10.67$, the smallest value of $U$ for which the equilibrium state is a single-phase nematic. For $\Gamma \geq 25$ the steady-state values are shown, while for $\Gamma < 25$—where the stresses oscillate indefinitely—the values shown are averages over an integral number of cycles of the oscillation. In the latter calculations, the first few cycles of oscillation were left out of the average, so that the starting state does not affect the average. $N_1$ computed in this way is positive at low $\Gamma$ ($0 \leq \Gamma \leq 7.5$), negative at intermediate $\Gamma$ ($8 \leq \Gamma \leq 67$), and positive again at large $\Gamma$ ($\Gamma \geq 70$). The first change in sign occurs in the tumbling regime, while the second occurs at a value of $\Gamma$ for which a steady state exists. Marrucci and co-workers obtained similar results for their two-dimensional calculations with the Maier–Saupe potential.[5,26] In Marrucci and Maffettone's calculations, for liquid crystalline phases with values of $U$ between $U^* = 2$ and 2.41, there is no tumbling at small $\Gamma$, and $N_1$ is positive at all shear rates. In this range of $U$, $S^{eq}$ is less than 0.5 or so, which is too low for tumbling to occur (see section IV.B). For the Onsager potential in three dimensions, we have noted that the minimum value of $U$ for the existence of an equilibrium liquid crystalline phase is 10.67, and the corresponding minimum value of $S^{eq}$ is 0.792, a value consistent with the measurements of Abe and Yamazaki on solutions of poly($\gamma$-benzyl L-glutamate) (PBLG) in dimethylformamide.[27] As we have seen, tumbling is predicted for this value or greater values of $S^{eq}$. Thus we predict that even for the lowest concentration at which an equilibrium nematic phase exists, there is tumbling at low shear rates and negative $N_1$ over a range of shear rates. However, the dependence of $N_1$ on $\Gamma$ predicted by Marrucci and Maffettone for $U$ just above $U^*$ agrees qualitatively with measurements of Kiss and Porter[2] for a PBLG sample whose concentration $c$ was reported to lie slightly above the minimum value $c_2$ required for formation of a completely liquid crystalline sample. We have no clear explanation for the discrepancy between our calculations using the Onsager potential and the measurements of Kiss and Porter in this concentration regime; molecular flexibility and polydispersity present in the experimental samples and absent from our calculations are possible sources of the discrepancy. Since the optical method used by Kiss and Porter to locate the concentration $c_2$ has been reported to be less than completely reliable,[28] it is also possible that the sample in question was really not completely liquid crystalline. Further work is needed

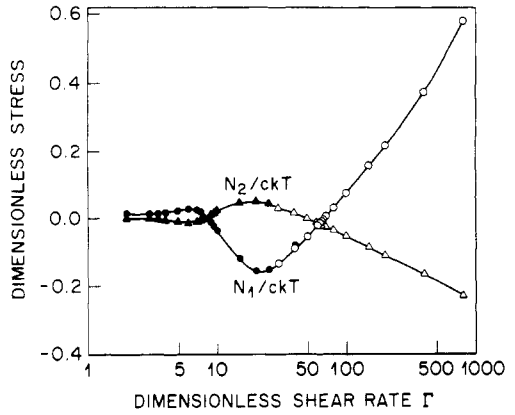


**Figure 12.** Dimensionless first and second normal stress differences $N_1/ckT$ and $N_2/ckT$ as functions of dimensionless shear rate $\Gamma$. The symbols are defined in the caption for Figure 9.

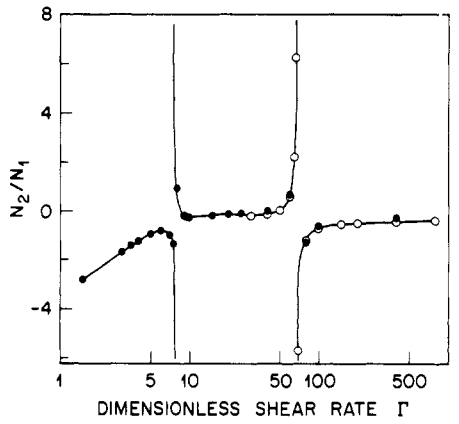


**Figure 13.** Ratio $N_2/N_1$ of the first to the second normal stress differences as a function of dimensionless shear rate $\Gamma$.

to clarify the situation.

The shear stress plotted in Figure 11 has a weak minimum at $\Gamma \approx 10$, which is in the wagging regime. At higher shear rates, from $\Gamma \approx 15$ up to $\Gamma = 800$, the shear stress $\sigma_{xz}$ is well approximated by a power law, $\sigma_{xz} \propto \Gamma^{0.12}$.

Our three-dimensional calculations also make possible the prediction of the second normal stress difference $N_2$. $N_2$ in the tumbling and wagging regimes is calculated by averaging the instantaneous value of $N_2$ over an integer number of cycles of the tumbling or wagging, as was done to obtain $N_1$. For fluids that are isotropic at equilibrium, $N_2$ has always been found to be negative or zero[29,30] and considerably smaller in magnitude than $N_1$. Figure 12 shows values $N_1$ and $N_2$ calculated as functions of shear rate $\Gamma$ for $U = 10.67$. $N_2$ is opposite in sign to $N_1$ except at shear rates close to those at which $N_1$ changes sign. Figure 13 plots the ratio $N_2/N_1$ as a function of $\Gamma$ at $U = 10.67$. In the low-shear-rate regime of positive $N_1$, $N_2$ is predicted to be negative and comparable in magnitude to $N_1$, which is consistent with preliminary measurements of $N_2$ and $N_1$ for liquid crystalline PBLG.[31]

Figure 14 summarizes the ranges of shear rate over which the first and second normal stress differences have positive or negative sign and the ranges over which the birefringence axis tumbles, wags, or comes to a steady-state orientation for $U = 10.67$.

Figure 15 is a plot of $N_1$ and $\sigma_{xz}$ for the dimensionless concentration $U = 12$. For this concentration, tumbling persists up to $\Gamma = 22$, wagging exists for $30 \leq \Gamma \leq 70$, and steady-state flow exists for $\Gamma \geq 100$. The relationships between these regimes and the regimes of positive and negative $N_1$ are similar to those found for $U = 10.67$. For

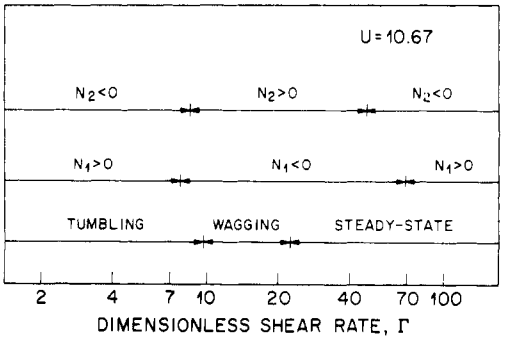


**Figure 14.** Regimes of dimensionless shear rate $\Gamma$ in which tumbling, wagging, or steady-state orientation of the birefringence axis occurs and in which the normal stress differences are positive or negative.

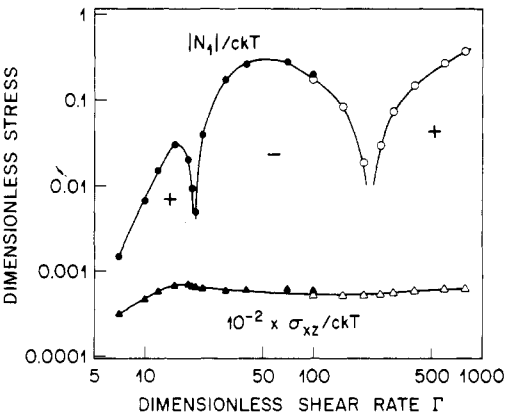


**Figure 15.** Dimensionless shear stress $\sigma_{xz}/ckT$ and first normal stress difference $N_1/ckT$ as functions of dimensionless shear rate $\Gamma$ for a dimensionless concentration $U$ of 12. The symbols are defined in the caption for Figure 9.

$U = 12$, just as with $U = 10.67$, $N_2$ has a sign opposite that of $N_1$ except at shear rates close to those for which $N_1$ changes sign.

## VII. Summary

The numerical results presented here confirm the main conclusion that Marrucci and Maffettone reached using their two-dimensional calculations, namely, that shearing at a high enough rate can significantly distort the orientation-distribution function, making it *less* anisotropic. This both arrests the tumbling of the major axis of the birefringence tensor that occurs at low shear rates $\Gamma$ and produces steady-state negative values of the first normal stress difference $N_1$. A transition to steady-state positive $N_1$ occurs when $\Gamma$ is increased enough that the effects of the excluded-volume potential are swamped by the flow effects.

Our time-dependent three-dimensional calculations supplement the results of Marrucci and Maffettone in that we also predict a regime in which the major birefringence axis wags around a fixed direction; this wagging regime occurs at shear rates intermediate between the tumbling and steady-state regimes.

We also predict the second normal stress difference $N_2$ and find that when $N_1$ has a steady-state value, $N_2$ is usually much smaller in magnitude than $N_1$ and opposite in sign; there is, however, a small region of shear rates in which the steady-state values of both $N_1$ and $N_2$ are negative.

At shear rates for which the major axis of the birefringence tensor wags or tumbles, we average the time-dependent stresses over an integral number of cycles of

the oscillation. The first normal stress difference obtained in this way changes sign from positive to negative as $\Gamma$ in increased, in qualitative agreement with the experimentally measured values. This behavior has also been reported by Marrucci and co-workers[26] in their two-dimensional calculations. In the lowest shear-rate regime in which the averaged value of $N_1$ is positive, we find the averaged value of $N_2$ to be negative and comparable to or greater in magnitude than the averaged value of $N_1$.

We also compute the effect of shear on the steady-state rheological properties of solutions of rodlike polymers that are isotropic at equilibrium. We find for the Onsager excluded-volume potential that shear can induce a discontinuous transition to a nematic phase only if the concentration is so high that the isotropic phase becomes metastable at equilibrium, the stable equilibrium being that of coexisting nematic and isotropic phases. This result may explain why shear-induced transitions have not been seen experimentally in lyotropic solutions.

## References and Notes


(1) Kiss, G.; Porter, R. S. *J. Polym. Sci., Polym. Symp.* **1978**, *No. 65*, 193.
(2) Kiss, G.; Porter, R. S. *J. Polym. Sci., Polym. Phys. Ed.* **1980**, *18*, 361.
(3) Navard, P. *J. Polym. Sci., Polym. Phys. Ed.* **1986**, *24*, 435.
(4) Moldenaers, P.; Mewis, J. *J. Rheol.* **1986**, *30*, 567.
(5) Marrucci, G.; Maffettone, P. L. *Macromolecules* **1989**, *22*, 4076.
(6) Doi, M. *J. Polym. Sci., Polym. Phys. Ed.* **1981**, *19*, 229.
(7) Onsager, L. *Ann. N.Y. Acad. Sci.* **1949**, *51*, 627.
(8) Maier, W.; Saupe, A. *Z. Naturforsch.* **1958**, *13A*, 564; **1959**, *14A*, 882; **1960**, *15A*, 287.
(9) Marrucci, G.; Ciferri, A. *J. Polym. Sci., Polym. Lett. Ed.* **1977**, *15*, 643.
(10) Thirumalai, D. *J. Chem. Phys.* **1986**, *84*, 5869.
(11) Mead, D. W.; Larson, R. G. *Macromolecules* **1990**, *23*, 2524.
(12) See, H.; Doi, M.; Larson, R. G. *J. Chem. Phys.* **1990**, *92*, 792.
(13) Doi, M.; Edwards, S. F. *J. Chem. Soc., Faraday Trans. 2* **1978**, *74*, 918.
(14) Doi, M.; Edwards, S. F. *The Theory of Polymer Dynamics*; Oxford University Press: New York, 1986.
(15) Larson, R. G. In *Recent Developments in Structural Continua*; Longman: London, 1990; Vol. 2.
(16) Lekkerkerker, H. N. W.; Coulon, P.; van der Haegen, R.; Deblieck, R. *J. Chem. Phys.* **1984**, *80*, 3427.
(17) Kuzuu, N.; Doi, M. *J. Phys. Soc. Jpn.* **1984**, *53*, 1031.
(18) Hinch, E. J.; Leal, L. G. *J. Fluid Mech.* **1976**, *76*, 187.
(19) Gähwiller, C. H. *Phys. Rev. Lett.* **1972**, *28*, 1554.
(20) Carlsson, T. *Mol. Cryst. Liq. Cryst.* **1984**, *104*, 207.
(21) Frank, R. C. *Discuss. Faraday Soc.* **1958**, *25*, 19.
(22) Mewis, J.; Moldenaers, P. *Mol. Cryst. Liq. Cryst.* **1987**, *153*, 291.
(23) Moldenaers, P. Ph.D. Thesis, Katholiecke Universiteit Leuven, 1987.
(24) Larson, R. G.; Mead, D. W. *J. Rheol.* **1989**, 33, 185.
(25) Hill, R. *Proc. Phys. Soc. London* **1952**, *A65*, 349.
(26) Marrucci, G. Presentation at the 61st Annual Meeting of the Society of Rheology, Montreal, Canada, Oct 21-26, 1989.
(27) Abe, A.; Yamazaki, T. *Macromolecules* **1989**, *22*, 2145.
(28) Wee, E. L.; Miller, W. G. *J. Phys. Chem.* **1971**, *75*, 1446.
(29) Keentok, M.; Georgescu, A. G.; Sherwood, A. A.; Tanner, R. I. *J. Non-Newtonian Fluid Mech.* **1980**, *6*, 303.
(30) Ramachandran, S.; Gao, H. W.; Christiansen, E. B. *Macromolecules* **1985**, *18*, 695.
(31) Magda, J. J.; Baek, S.-G.; de Vries, L.; Larson, R. G., manuscript in preparation.


# Relaxation of Entangled Polymers in Melts


**J. des Cloizeaux**

*Service de Physique Théorique† de Saclay, 91191 Gif-sur-Yvette Cedex, France*



*Received July 31, 1989; Revised Manuscript Received November 1, 1989*



ABSTRACT: In this paper, a theoretical study of the relaxation of entangled polymers in melts is presented, the aim being to reproduce experimental results in a precise manner. The reptation concept introduced by de Gennes is used for this purpose but with strong modifications. Several results are obtained. First, a phenomenological approach is used to confirm the validity of the "double reptation" principle that enables us to deduce the relaxation of a mixture of very long polymers and of moderately long polymers from the relaxation of each species considered separately. This assumption being well verified, the problem reduces to the relaxation of monodisperse polymers. Then, it is shown that the relaxation of such polymers can be deduced from the motions of stress points on the chains. It is assumed that the diffusion constant of a point depends on its position on the chain. Moreover, the fact that sliding motion as well as diffusive motion may simultaneously contribute to reptation is taken into account. Three related models are presented, exactly solved, and discussed. One model gives results in good agreement with experiments (on polybutadiene), and this model, which incorporates diffusion and sliding effects, is especially simple from a mathematical point of view since it belongs to a class of easily tractable models whose study seems promising.


## I. Introduction

In order to describe relaxation processes in polymer melts made of long polymers, P.-G. de Gennes[1] introduced the reptation concept in 1971, and this idea was later developed by M. Doi and S. F. Edwards.[2] Our problem here is to calculate the stress relaxation function $G(t)$ (where $t$ is time), but in practice the experimentalists measure $G''(\omega)$ and $G'(\omega)$.

$$G''(\omega) = \omega \int_0^\infty dt \cos \omega t\, G(t) \quad \text{(loss modulus)}$$

$$G'(\omega) = \omega \int_0^\infty dt \sin \omega t\, G(t) \tag{1}$$

Simple diffusion reptation can be used in the context of the tube model to obtain an expression for $G(t)$. After time $t$, a part of the initial tube remains unchanged; let

† Laboratoire de l'Institut de Recherche Fondamentale du Commissariat à l'Energie Atomique.


0024-9297/90/2223-3992$02.50/0